Title

Investigation on the electron flux to the wall in the VENUS ion source

Journal

Review of Scientific Instruments, 87(2)

ISSN

0034-6748

Authors

Thuillier, T

Angot, J

Benitez, JY

et al.

Publication Date

2016-02-01

DOI

10.1063/1.4935989

Peer reviewed

Investigation on the electron flux to the wall in the VENUS ion source

T. Thuillier, J. Angot, J. Y. Benitez, A. Hodgkinson, C. M. Lyneis, D. S. Todd, and D. Z. Xie

Citation: Review of Scientific Instruments **87**, 02A736 (2016); doi: 10.1063/1.4935989
View online: https://doi.org/10.1063/1.4935989
View Table of Contents: http://aip.scitation.org/toc/rsi/87/2
Published by the American Institute of Physics

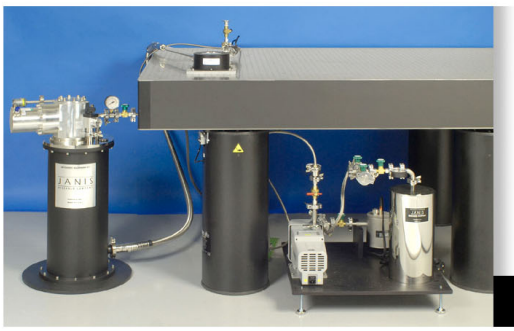

Investigation on the electron flux to the wall in the VENUS ion source

T. Thuillier,[1,a)] J. Angot,[1] J. Y. Benitez,[2] A. Hodgkinson,[2] C. M. Lyneis,[2] D. S. Todd,[2] and D. Z. Xie[2]
[1]*LPSC, Université Grenoble-Alpes, CNRS/IN2P3, 53 rue des Martyrs, 38026 Grenoble Cedex, France*
[2]*Nuclear Science Division, Lawrence Berkeley National Laboratory, Berkeley, California 94720, USA*

(Presented 25 August 2015; received 5 September 2015; accepted 4 November 2015; published online 1 December 2015)

The long-term operation of high charge state electron cyclotron resonance ion sources fed with high microwave power has caused damage to the plasma chamber wall in several laboratories. Porosity, or a small hole, can be progressively created in the chamber wall which can destroy the plasma chamber over a few year time scale. A burnout of the VENUS plasma chamber is investigated in which the hole formation in relation to the local hot electron power density is studied. First, the results of a simple model assuming that hot electrons are fully magnetized and strictly following magnetic field lines are presented. The model qualitatively reproduces the experimental traces left by the plasma on the wall. However, it is too crude to reproduce the localized electron power density for creating a hole in the chamber wall. Second, the results of a Monte Carlo simulation, following a population of scattering hot electrons, indicate a localized high power deposited to the chamber wall consistent with the hole formation process. Finally, a hypervapotron cooling scheme is proposed to mitigate the hole formation in electron cyclotron resonance plasma chamber wall. [http://dx.doi.org/10.1063/1.4935989]

I. DAMAGE TO THE PLASMA CHAMBER

The long-term operation of high charge state electron cyclotron resonance ion sources (ECRISs) fed with high microwave power has caused damage to the plasma chamber wall in several laboratories. On the VENUS ECRIS,[1] slow metal erosion was observed over a few year time scale at the place where the magnetic field intensity to the wall is the weakest. The hole was formed on the injection flute at $\mathbf{z} = -45$ mm with respect to the plasma chamber center (see Figure 1). Metal analysis has shown that the aluminum alloy recrystallized and became porous. The temperature required to favor this process is approximately 300 °C that could be reached when the power flux to the wall exceeds the so called critical heat flux (CHF) limit of ~1 MW/m^2.[2,3] Despite an efficient flute-channel cooling fed with 6 bars water at 25 °C and a fluid velocity of 9 m/s, the power flux imbalance makes the wall temperature increase above 150 °C when steam bubbles are created. With stationary bubbles, the wall dries and the heat exchange coefficient decreases, making the wall temperature to increase further to reach the equilibrium. In ECRIS, the radio frequency (RF) power injected into the plasma is mainly transferred to the electrons. The ions are cold and do not contribute significantly to the power balance. The paper describes the interaction of the hot electrons with the chamber walls. In Section II, the microscopic effects influencing the motion of electron in the magnetic field are reviewed. Section III presents a first geometrical model to estimate the power flux at wall. Section IV covers the result of a Monte Carlo simulation resulting in a high localized power density at wall. Section V explores the option to use hypervapotron cooling to tackle the CHF limit observed in third generation ECRIS.

II. ELECTRON SCATTERING IN AN ECRIS PLASMA

The plasma hot electrons are strongly magnetized and confined in ECRIS. The minimum-B field configuration, resulted from the superimposition of axial magnetic mirrors and radial hexapole fields, confines the charged particles with lifetime up to milliseconds. The magnetic mirror ratios $\boldsymbol{R} = \boldsymbol{B_{max}}/\boldsymbol{B_{min}}$ between 2 chamber walls derived from Figure 1 are spanning from 6.4 to 3.8 and the associated limit theta pitch angles $\boldsymbol{\theta}$ (where particles become deconfined) are ranging from 23° to 31°. At low to intermediate energy, the electron confinement is improved when it gains energy passing through the ECR zone. The mechanisms, which cause deconfinement of those electrons, are the Coulomb collision and the electron impact (EI) with ion. At higher energy, the electrons are deconfined by the RF scattering.[4] In this section, the different mechanisms affecting the electron trajectories are reviewed and estimated in the ECRIS plasma.

A. Coulomb collision

The Coulomb scattering (CS) of electrons with the charged particles in a plasma having an electron temperature $\boldsymbol{kT_e}$ and a mean ion charge state $\boldsymbol{Z}$ is estimated by the mean (momentum) electron collision frequency with ions $\langle \boldsymbol{\nu_{ei}} \rangle$ and electrons $\langle \boldsymbol{\nu_{ee}} \rangle$,[4]

Note: Contributed paper, published as part of the Proceedings of the 16th International Conference on Ion Sources, New York, New York, USA, August 2015.
a)Electronic mail: thuillier@lpsc.in2p3.fr.

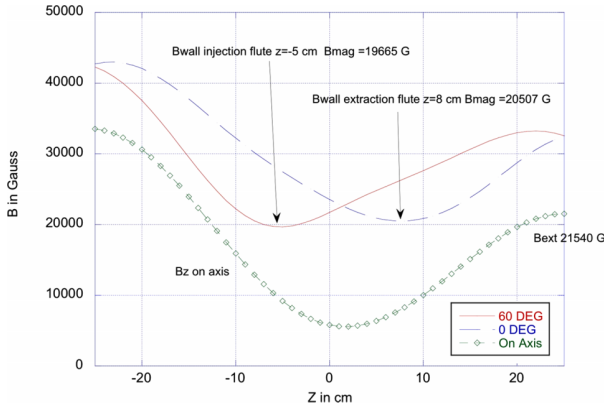

FIG. 1. Diamonds: Axial magnetic field on axis. Solid and dashed lines: Magnetic field intensity at the wall along two consecutive hexapole magnetic flutes.

$$\langle \nu_{ei} \rangle = \frac{2^{1/2} n_i Z^2 e^4 \ln \Lambda}{12\pi^{\frac{3}{2}} \epsilon_0^2 m_e^{\frac{1}{2}} (kT_e)^{3/2}}, \tag{1}$$

$$\langle \nu_{ee} \rangle \approx \frac{\langle \nu_{ei} \rangle}{n_i Z^2 / n_e}, \tag{2}$$

where n_i and n_e are the ion and electron density, $-e$ is the negative electron electric charge, $\ln \Lambda$ is the Coulomb logarithm, ϵ_0 is the vacuum permittivity, and m_e is the electron mass. Eqs. (1) and (2) correspond to the mean frequency of multiple low angle Coulomb scattering resulting in a total scattering angle of 90°. Eq. (1) is valid for a Gaussian distribution of electrons at a temperature T_e interacting with cold ions. In ECRIS plasma, it is commonly accepted that 3 different electron populations co-exist:[5] a cold electron population associated with the plasma potential and the secondary electron emission from the wall, a quasi-Maxwellian warm electron distribution with a temperature measured around ~1 keV, and an anisotropic hot relativistic energy tail.[6] The relative weight of each population is not known precisely. In this study, the mean electron temperature used to estimate the electron collision frequency is assumed to be 5 keV. The other parameters necessary to estimate the collision frequency are taken as follows. The Coulomb logarithm is estimated to ~10 and the electron density of the fully ionized plasma is taken as $\sim 10^{13}$ cm^{-3}, the cutoff density when the plasma is heated with 28 GHz microwaves. The chamber failure occurred when the source was tuned for a high charge state xenon plasma with a mean charge state Z ~ 22. The electron Coulomb collision, which occurs in the Debye sphere, is understood as a tiny random deviation of the electron velocity per unit time. Thus, a large scale change of direction requires a very large number of small angle collisions. The electrons are expected to have their pitch angle θ slowly varying with time and moving toward the loss cone. The characteristic times τ_{ei} and τ_{ee} for an electron to scatter by 90° are included in Table I as a function of its kinetic energy. The dominant effect is electron–ion scattering here. Electron-electron scattering is neglected in the next study.

B. Electron impact

The EI collision of an energetic electron with an ion causes the impinging electron to loose energy, but also to redistribute randomly its velocity direction. In this process, the electron comes close to the ion nuclei and undergoes a subsequent deep Coulomb interaction which can change the electron velocity direction by 90°. So, the EI has to be considered as far as electron de-confinement is concerned. The time scale τ_{EI} for this process is estimated using the Lotz empirical cross section σ_{EI}[7] for a Xe^{22+} creation considering $\tau_{EI} \sim 1/(\sigma_{EI} n_i v_e)$, v_e being the impinging electron velocity. In the plasma of interest, the time for EI is much larger than the time for CS.

TABLE I. Characteristic time for electron diffusion in the plasma.

Kinetic energy (keV)	1	5	10	100
$\tau_{ei} \sim 1/\langle \nu_{ei} \rangle$ (ms)	0.005	0.054	0.15	5
$\tau_{ee} \sim 1/\langle \nu_{ee} \rangle$ (ms)	0.11	1.22	3.45	109
$\tau_{RF} \sim 1/\langle \nu_{RF} \rangle$ (μs)	∞	∞	∞	~2-3
$\tau_{EI} \sim 1/(\sigma_{EI} n_i v_e)$ (ms)	1.11	0.45	0.48	0.93
τ_{DRIFT} (ms)	~0.001	~0.005	0.002	0.0002

C. Radio frequency scattering

The microwave injected in the ECRIS can couple to the whistler mode whose wave vector k is parallel to the local magnetic field B.[8] The RF scattering in an ECRIS plasma has been studied by Girard[9] to estimate the mean electron velocity kick parallel ($\delta v_{\parallel}$) and perpendicular ($\delta v_{\perp}$) to the magnetic field when it crosses the ECR zone,

$$\delta v_{\parallel} = \frac{eE}{m_e} \frac{v_{\perp}}{v_{\phi}} \sqrt{\frac{\pi}{\omega' v_{\parallel}}}, \tag{3}$$

$$\delta v_{\perp} = \frac{eE}{m_e} \left(1 - \frac{v_{\parallel}}{v_{\phi}}\right) \sqrt{\frac{\pi}{\omega' v_{\parallel}}}. \tag{4}$$

E is the electric field intensity, v_{ϕ} is the phase wave velocity, and ω' is the derivative of the local electron cyclotron frequency $\omega = eB/m_e$ along the magnetic field B. The above equations are used to estimate the time τ_{RF} for the electron theta pitch to be tilted by 90° as a function of its kinetic energy. As expected, the RF scattering improves the electron confinement when $v_e \ll v_{\phi}$. The deconfinement process is estimated to start above ~25 keV for $\frac{v_{\phi}}{c} \sim 0.45$. This last value being estimated from Girard and with typical numbers for the VENUS plasma. In the present study, the RF scattering is not considered. The hot electron tail is neglected with respect to the warm electrons population responsible for the ion ionizations. Anyway, the RF scattering process is expected to scatter slowly the electron like the CS. The lost to the wall induced by the RF for hot electrons is likely to be similar to the CS considered with warm electrons.

D. Drift velocity

There are two distinct regions in an ECRIS as far as particle trajectories are concerned. The first region is a cylinder centered around the chamber axis. There, the hexapole magnetic field intensity is negligible with respect to the axial one; the field lines are slightly bent and the magnetic gradient does not exceed 10 T/m. The electron trajectories are very

stable there. In the second region, located around this central tube, the hexapole magnetic field gradient becomes much stronger (up to ~60 T/m at wall) and the field lines are strongly bent toward the wall (bending radius $\boldsymbol{R} \sim 0.1$ m). There, the electrons motion undergoes drift velocities resulting in a quite rapid scattering from a magnetic pole to another. The drift velocity expression due to the magnetic gradient and the field line curvature is[10]

$$\overrightarrow{v_D} = -\frac{m_e {v_\perp}^2}{2eB^3}\vec{B} \times \vec{\nabla}\vec{B} - \frac{m_e {v_{||}}^2}{R^2 eB^2}\vec{R} \times \vec{B}. \quad (5)$$

The two drift contributions, related through the Maxwell equations, have the same order of magnitude in ECRIS. The time τ_D for an electron to drift azimuthally by 360° in the peripheral region can be roughly estimated by $\tau_D \sim 2\pi r/v_D$, with r taken as the half radius of the plasma chamber accounted from the source axis. For 1 keV electrons, τ_D is of the order of the μs, which is much smaller than the collision time as seen in Table I. This means that peripheral electrons are spending their time roaming along the whole hexapole field lines connected to the cylinder wall. Because the Coulomb scattering is much longer, this roaming is likely to make the majority of electrons impinge the wall where the magnetic mirror intensity is the weakest.

III. MAGNETIC FIELD LINE MODEL

As a first approach, the heating power distribution to the wall is studied using a simple geometrical model based on the study of the field lines passing through the ECR zone and impinging the chamber walls. This hypothesis is validated by the fact that electrons are strongly magnetized in the non-collisional ECRIS plasma. The surface created by the field lines intersecting the wall is used to estimate the power density to the wall. Helped with a 3 dimensional magnetic field map of the cylindrical VENUS plasma chamber, the ECR zone surface is meshed into a set of 1 mm^2 elementary triangles. Next, the magnetic field line passing through each individual triangle edge is computed and followed on both sides until it reaches the plasma chamber wall, either radially or axially. Information on the field lines geometry and magnetic intensities is stored for further analysis. The plasma chamber wall is cut into three surfaces: the injection plane ($z = -250$ mm), the extraction plane ($z = 250$ mm), and the cylinder wall ($r = 71.4$ mm and $|z| < 250$ mm).

The electron flux $\boldsymbol{F}$ to the wall is weighted for each field line by a set of factors to estimate at best the power density at wall. It is generally thought that the dense plasma in an ECRIS is located inside the closed ECR zone. In this model, it is assumed that the electron density is uniform inside the ECR zone and that the field lines have approximately all the same mirror ratios. Under these assumptions, the number of electrons populating a particular field line is proportional to its length. So the first weighting considered is the part of the magnetic field line length $\boldsymbol{L_i}$ included in the ECR zone. The second weighting considered is the magnetic field intensity at wall. The magnetic field confinement acts as a "leaky box" where the particles are mostly escaping by the weakest magnetic intensity point. If we consider the magnetic pressure for a plasma of density $\boldsymbol{n}$, we get $\boldsymbol{P} = \boldsymbol{B}^2/2\mu_0 \sim \boldsymbol{nkT}$. The differentiation gives $\Delta \boldsymbol{n} \sim \Delta \boldsymbol{B} = (\boldsymbol{B_{max}} - \boldsymbol{B_i})$, where $\boldsymbol{B_{max}}$ and $\boldsymbol{B_i}$ are, respectively, the maximum and the local magnetic field intensity at wall. It is expected that plasma regions with a high density should leak toward region with the weakest magnetic field; the flux of particle to the wall is thus assumed to be proportional to $(\boldsymbol{B_{max}} - \boldsymbol{B_i})$. The total power to the wall is finally calculated as follows:

$$\boldsymbol{P_{tot}} = \sum_{i=1}^{N} \boldsymbol{F_i dS_i}, \quad (6)$$

$$\boldsymbol{F_i} = \boldsymbol{f L_i (B_{max} - B_i)}, \quad (7)$$

with N the total number of triangles, $\boldsymbol{dS_i}$ the local triangle surface, $\boldsymbol{f}$ a normalization coefficient. The local power density is such that

$$\frac{\boldsymbol{dP}}{\boldsymbol{dS}} = \boldsymbol{F_i}. \quad (8)$$

In the case of VENUS, the chamber burnout occurred with a total power of 4 kW and this power is used to determine $\boldsymbol{f}$. The result of the computation is summarized in Table II and displayed in Figure 2. It is noticeable that the model predicts a peak power density above the CHF of 1 MW/m^2 along the injection flute at the wall. The peak power position is found at $z = -74$ mm (see the black dashed line in the upper part of Fig. 2) while it is experimentally measured at −45 mm. The model is too crude to predict the accurate peak power position. The white area visible in the center of the extraction plot (Fig. 2 bottom right) corresponds to the extraction electrode hole. No electrons are expected to cross this area where a high voltage electrical field is used to accelerate the ions and repels the electrons. It is also noticeable that the density plots in Fig. 2 are very similar to the observed plasma marks in ECRIS.

IV. MONTE CARLO SIMULATION

The investigation continues with a 3-d Monte Carlo simulation in which hot electron trajectories are followed until they touch the wall. The simulation includes the Coulomb scattering and the electron impact collisions. The spatial distribution of incident electron is chosen to match a uniform electron density in the ECR zone. The electron initial pitch angle is chosen to grant its magnetic confinement. The electrons are tracked using a Boris scheme leapfrog algorithm.[11] The time interval to solve the equations of motion is chosen to grant numerically stable trajectories above 1 ms. The particle velocity is randomly scattered at each cyclotron turn by a tiny angle $\boldsymbol{\delta\theta}$ calculated according to Eq. (1). The probability to

TABLE II. Estimated power deposited on the ion source wall by the geometrical simulation.

	Injection	Extraction	Cylinder
Surface (cm^2)	7.7	10.7	106.3
Power deposited (%)	3.2	10.6	86.2
Power deposited (W)	127	426.3	3446.7
Peak power density (kW/m^2)	348	948	1085
Location of the peak power			Z =−74 mm

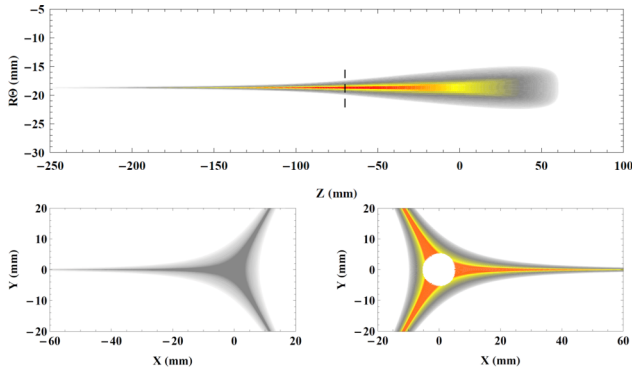

FIG. 2. Top: Power density to the cylinder wall on an injection flute. Bottom: Power density deposited on the injection (left) and extraction (right) planes. The power density increases with the colors in the following order: white (0), gray, yellow, red (1.1 MW/m^2).

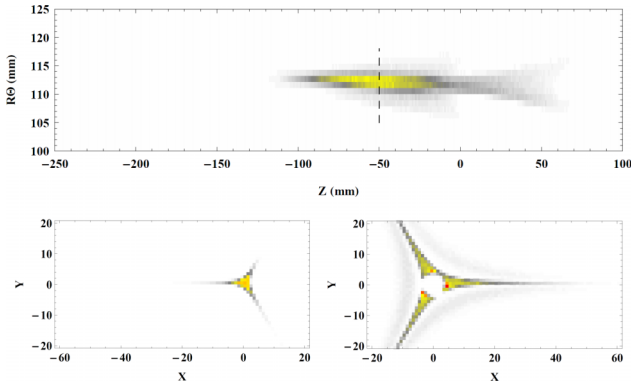

FIG. 3. Top: Power density to the cylinder wall on the pole 2. Bottom: Power density deposited on the injection (right) and extraction (left) planes. The power density increases with the colors in the following order: white (0), gray, yellow, red (4.6 MW/m^2).

get an EI is also randomly evaluated which resulted in a large 45° pitch angle scattering. The extraction electrode hole with an 8 mm diameter is modeled as a perfect electron reflector, since the electric field, present in this area to extract ions, repels electrons back to the source. The electron kinetic energy in the simulation is chosen to be 5 keV, well below the source high voltage (20–30 kV). The simulation includes the experimental plasma chamber position offset with respect to the magnetic field. The offset is, respectively, 0.5 and 0.7 mm along X and Y directions, Z being the source axis. The result of the Monte Carlo simulation is synthesized in Table III and plotted in Figure 3 when the pixel size is set to 1 mm^2.

With a total deposited power of 4 kW, it is striking to note that the power density along the flute reaches up to 3.1 MW/m^2. The highest power density of 4.6 MW/m^2 is located on 3 tiny spots very close to the extraction electrode hole. Erosion of extraction electrode has been observed in many laboratories, but this massive part is easy to cool and replace in case of failure. The very small pattern found on the injection plane is interpreted as an image of the electron population efficiently reflected by the high voltage extraction system. The size of this pattern is smaller than the plasma electrode diameter of 8 mm. As expected, the highest power flux to the cylinder wall goes where the magnetic field intensity is the weakest (pole 2). It is striking to note that the tiny chamber offset unbalances the flux density to the even poles by ~14%. The flux imbalance for the odd poles reaches 40%. The total surface impacted by electron is 149 cm^2, larger by 25 cm^2 to the one found

TABLE III. Estimated power deposited on the ion source wall by the Monte Carlo simulation with a 1 mm^2 pixel size.

	Surface (cm^2)	Power deposited	Peak power density (MW/m^2)
Injection	1.3	73	3.4 ± 0.1
Extraction	18.2	425	4.6 ± 0.1
Pole 1	23.2	546	1.6 ± 0.1
Pole 2	22.0	754	3.0 ± 0.1
Pole 3	23.9	604	2.0 ± 0.1
Pole 4	19.7	591	3.1 ± 0.1
Pole 5	21.6	449	1.3 ± 0.1
Pole 6	19.3	558	2.6 ± 0.1
Total	149.2	4000	

with the previous field line model. Despite a larger surface covered, the power density to the wall is found 3 times higher with the Monte Carlo than with the field line model. Here, a large portion of the surface of impact corresponds to a low electron flux, while narrow surfaces get the highest flux. Figure 4 shows the local histogram plot of power density on the flute 2 along Z (top) and Rθ direction (bottom), with particles selected to impinge close to the peak ($37.3 < R\theta < 37.5$ mm and $-60 < z < -40$ mm). With a histogram bin size of 0.05 mm, the power density appears very localized along the Rθ direction where a narrow peak thinner than 1 mm can be seen right on the theoretical pole axis. The power distribution is broader and quasi-Gaussian along Z with a root mean square of 19 mm. The maximum peak density on the wall goes up to 5 MW/m^2 for z = −49 mm which is close to the experimental hole position found at −45 mm. The power flux remains high and nearly constant for −60 < z < −40 mm. As the cooling water flows toward the positive Z direction, the water temperature increases toward the positive Z which suggests a higher wall temperature for z > −49 mm. This effect could explain the 4 mm position discrepancy between simulation and measurement.

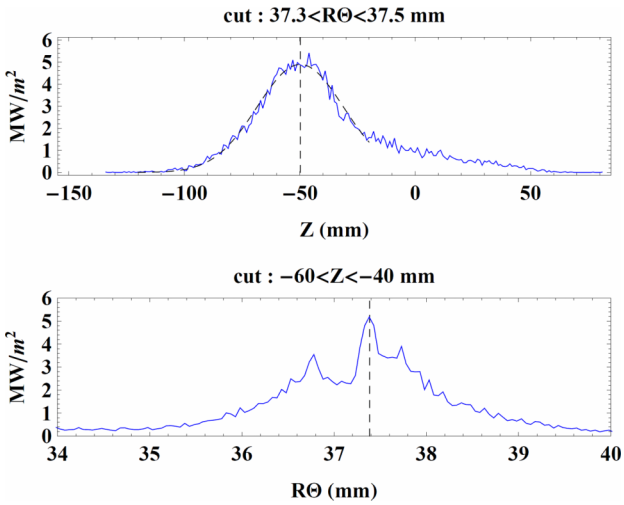

FIG. 4. Histogram plots along Z (top) and Rθ (down) of the power density near to the peak power location along flute 2. A sharp peak reaching 5 MW/m^2 is observed right at the theoretical pole position.

V. PROSPECTS TO IMPROVE CHAMBER COOLING

For the 3rd generation sources such as VENUS, there are straightforward ways to improve the cooling to prevent chamber burnout. For example, the aluminum wall thickness where burnout occurred was only 2 mm and this was too thin to provide sufficient lateral heat flow away from the localized heating. A new chamber is in operation, which addresses this. Still, the constant need for higher beam intensity and higher charge state ions strongly motivates the development of the 4th generation of ECR ion sources, which are anticipated to operate at much higher wave power of tens of kW. The plasma chamber failure which occurred in long-term operations of ECRIS must be addressed with care to assure the success of the next generation of ECR ion sources. Very high power density fluxes are well managed in several experimental fields, like microwave tubes, beam dumps, and tokamak divertors, thanks to the hypervapotron technique. Hypervapotron has been pioneered by C. Beutheret for cooling of anodes in high power tetrodes at Thomson CSF.[12] The effect has been visualized by Cattadori.[13] A clear and concise explanation of the hypervapotron principle is reproduced here for convenience[14] (see also Figure 5): "in this technique, fins are placed transverse to a forced fluid flow. The bulk fluid remains well subcooled. If the water between the fins is sufficiently stagnant, steam bubbles will grow inside the grooves and drive the warm water out. Once the steam bubble extends into the well subcooled bulk water, the bubble collapses and the colder bulk water is drawn into the groove where it re-wets the surfaces. This process allows operation with parts of the exchange surface at above the CHF. The rate of surface temperature rise during the steam phase is reduced by heat conduction into the cold fins." Hypervapotron uses a diphasic heat exchange and takes advantage of the fact that steam has a high heat flux capacity, provided the steam is rapidly replaced by a liquid in contact with the surface to cool. Hypervapotron's efficient cooling should be considered for the plasma chamber cooling, especially for the next generation ECRIS to ensure safe and reliable operations with possible tens of kW wave power needed. The hypervapotron thickness is of the order of 20 mm: the future magnetic structure should include an extra room in the cryostat warm bore to grant space for a hypervapotron cooled plasma chamber.

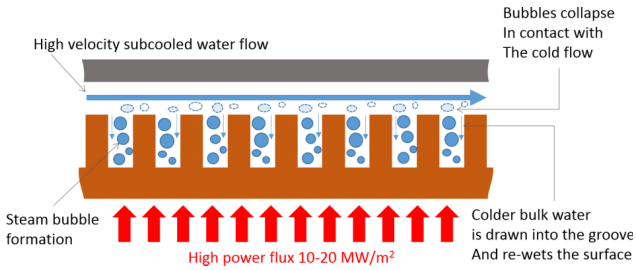

FIG. 5. Schematic showing the principle of the hypervapotron technique.

[1]C. Lyneis, D. Leitner, M. Leitner, C. Taylor, and S. Abbott, Rev. Sci. Instrum. **81**, 02A201 (2010).
[2]D. C. Woodcock, J. S. Gilbert, and S. J. Lane, J. Geophys. Res. **117**, B10205, doi:10.1029/2012JB009240 (2012).
[3]L. A. Bromley, N. R. LeRoy, and J. A. Robbers, Ind. Eng. Chem. **45**(12), 2639–2646 (1953).
[4]F. F. Chen, *Introduction to Plasma Physics and Controlled Fusion* (Plenum, 1984).
[5]G. Melin, F. Bourg, P. Briand, J. Debernardi, M. Delaunay, R. Geller, B. Jacquot, P. Ludwig, T. K. N'Guyen, L. Pin, M. Pontonnier, J. C. Rocco, and F. Zadworny, Rev. Sci. Instrum. **61**, 236 (1990).
[6]C. Barue, M. Lamoureux, P. Briand, A. Girard, and G. Melin, J. Appl. Phys. **76**(5), 2662 (1994).
[7]W. Lotz, Astrophys. J., Suppl. **14**, 207 (1967).
[8]T. H. Stix, *Waves in Plasmas* (American Institute of Physics, New York, 1992).
[9]A. Girard, C. Perret, G. Melin, and C. Lécot, Rev. Sci. Instrum. **69**, 1100 (1998).
[10]R. Dendy, *Plasma Physics: An Introductory Course* (Cambridge University Press, 1993).
[11]J. P. Boris, "Relativistic plasma simulation-optimization of a hybrid code," in *Proceedings of the 4th Conference on Numerical Simulation of Plasmas* (Naval Research Laboratory, Washington, DC, 1970), pp. 3–67.
[12]C. Beutheret, "Transfert de flux superieur a 1 kW/cm^2 par double changement de phase entre une paroi non isotherme et un liquide en convection forcee," in Proceedings of the International Heat Transfer Conference, Paris, 1970.
[13]G. Cattadori *et al.*, "Hypervapotron technique in subcooled flow boiling CHF," Exp. Therm. Fluid Sci. **7**, 230–240 (1993).
[14]H. D. Falder and E. Thomson, Fusion Sci. Technol. **29**(4), 584–595 (1996).